Laboratory Report
NRAO Electronics Division Internal Report Series
Report No. 317
July 17, 2006

A Low Cost Screened Enclosure for Effective Control of Undesired Radio Frequency Emissions

Richard F. Bradley

NRAO Technology Center, 1180 Boxwood Estate Rd., Charlottesville, VA 22903

Abstract. This report describes a low cost, shielded enclosure that was developed to contain the electromagnetic radiation generated by electronic equipment in order to reduce the potential for radio frequency interference (RFI). The enclosure is made from thin wire mesh screening that is attached to a wooden framework for support. Allowances are made at both ends of the enclosure for large cable bulkheads. A special seam was developed to maintain a low resistive current path between adjacent sections of screening. Lossy dielectric material is used inside to greatly reduce leakage resulting from the cavity resonance effect. The physical behavior of the enclosure is modeled and compared with laboratory based measurements. A plot of shielding effectiveness versus frequency is presented.

1. Introduction

The high degree of sensitivity and stability required for the statistical detection of weak, cosmic radio sources places strict limits on the emissions of electromagnetic radiation from nearby electronic equipment that can be tolerated during astronomical observations. The Green Bank Interference Protection Group (IPG) has adopted strict new emissions guidelines for any equipment located in close proximity to the Green Bank Telescope (GBT) (Beaudet *et al.* 2005). Compliance with this order requires that all such equipment be subjected to sensitive, calibrated field-strength measurements taken inside the Green Bank anechoic chamber.

Other radio astronomy instruments will also benefit from the added protection. For example, it is sometimes useful to locate signal processing equipment relatively close to sensitive receivers. Modern, high-speed digital electronics, necessary for wide-bandwidth signal processing applications from spectrometers to correlators, generate an excess of harmonic-rich, pulse-type emissions. Another example is regenerative feedback in wide-bandwidth, high-gain, non-heterodyne receivers that can lead to strong oscillations, gain instabilities, and uncontrolled correlation bias among array elements. In both cases, the problem can be managed through the application of proper RF shielding techniques that prevent such emissions from becoming RFI.

The most effective means by which to provide a degree of electromagnetic compatibility (EMC) among receiver sub-systems is to encapsulate the emitting electronics in a metallic enclosure to effectively isolate them from the sensitive RF components. Indeed, the control room housing the back-end electronics for the GBT is one such example. Radio frequency shielding techniques are

quite different from those intended for quasi-static electric fields. For example, an automobile provides its occupants with a measure of lightning protection, but does little to shield RF emissions. For electromagnetic radiation, any tiny hole in the enclosure will act as an aperture through which a small amount of radiation will escape. Walls made from solid materials are the most effective, but are very costly to manufacture. Ease of access to the enclosed equipment, the feed-through of wires and cables, and the need for adequate ventilation all tend to compound the RF shielding challenge and can potentially compromise the overall effectiveness of the structure by introducing unwanted apertures.

One approach to solving this problem is to use metallic mesh screening for the walls of the enclosure. It is relatively inexpensive, light weight, easily cut to required dimensions, readily attached to a framework, and allows for copious air flow. Such enclosures have been built in the past, but the degree of shielding effectiveness has varied greatly from one structure to another. Seams, door gaskets, bulkhead seals, and the screening material itself have all been suspect. It was apparent that the mechanism by which radiation leaks from such an enclosure was poorly understood.

This report presents the results of an investigation geared toward the physical mechanisms of RF leakage through metallic screened enclosures with the aim of applying this knowledge to develop an inexpensive, yet highly effective, approach to shielding. A suitable enclosure was fabricated and its shielding effectiveness characterized. The basic construction details of this prototype, together with an electromagnetic analysis of the structure, are presented in the following sections. The physical properties of the wire mesh and absorbing material were characterized by S-parameter measurements taken at 1.5 GHz and 3.5 GHz. Finally, the overall effectiveness of the enclosure was evaluated by careful spectral measurements taken in the Green Bank anechoic chamber.

2. Construction Details

A photograph of the enclosure is shown in Fig. 1. Basic construction notes are provided in this section with additional details and assembly instructions given in the Appendix. The inside dimensions were chosen to be 29 x 29 x 63 inches (73.7 x 73.7 x 160 cm), which is large enough to house a variety of electronic equipment. These specific dimensions can easily be attained from standard stock material sizes with minimal waste.

The fundamental shielding material is insect screening made from 0.011" (0.28 mm) diameter bronze wire woven into a rectangular mesh having a nominal 18 x 14 holes per inch (see Fig. 2). The largest aperture dimension is approximately 1.55 mm of $\frac{1}{38}\lambda$ at 2 GHz, where λ is the wavelength of the electromagnetic radiation. This screening should provide significant RF containment, yet be porous enough to allow adequate convective cooling. Note that the wires are physically touching one another at the cross-over points in the weave, but are not bonded in any way.

The screen wire that is attached to the inside of the framework, constructed from pieces of white pine having a 1.5 inch square, through stapling. Each side of the enclosure was assembled separately using bonded, double-lap joints with dowels to add strength and maintain squareness during fabrication. The sides

Figure 1. Photograph of the shielded enclosure. The top cover is removable. The wooden framework for one of the bulkheads is visible on the end.

were fastened together using No. 8 wood screws spaced along the framework on approximately 2 inch centers as shown in Fig. 1.

A low resistance connection is needed where two pieces of wire screening come together. Soldering and brazing techniques were not considered due primarily to the large amount of labor required. As an alternative, a special compression joint was designed for that purpose. Copper gauze is used as an electromagnetic gasket because it is pliable and can easily mold to fill small voids. Copper is adjacent to brass in the galvanic series (Van Vlack 1980) so that corrosion caused by composition cells is mitigated. Wood screws were used to press the copper gauze and screens together. A gentle, distributed compression of the metals along the entire length of the interface is ensured by incorporating fiberglass rope seal into the joint to eliminate gaping that may result from non-uniform wood surfaces or variations in the amount of force provided by the screws. *Care should be taken to remove all loose fragments of the copper gauze before electronic equipment is placed inside the enclosure to prevent unintentional electrical shorts.*

Two large bulkheads, each having an effective area of 9 x 21 inches (22.9 x 53.3 cm), were included in the design to accommodate cabling. Large feedthroughs with 1 μF of shunt capacitance are used to pass AC power. *It is important for safety reasons that a ground strap be connected between the metal screen of the enclosure and the ac power ground to prevent electrical shock caused*

by these capacitors. The capacitive reactance at 60 Hz is only approximately 2600 ohms. RF is passed using standard coaxial feed-through connectors. Digital LAN access is via fiber lines that pass through a 10 inch long section of 1/2 inch diameter copper tubing that is soldered to the bulkhead. It should be noted that these techniques are all quite common and have well-proven performance. The measurements described in this report were performed with no bulkheads in place in order to confine the study to the screen material and the interfaces.

3. Electromagnetic Behavior of Screen Wire

It may be shown that a small aperture in a thin metallic sheet that is placed along a plane perpendicular to the energy flow inside a metallic waveguide or coaxial cable will appear as an equivalent shunt inductance in a transmission line model (Marcuvitz 1951). That model may be used to analyze the amount of coupling between adjacent sections of liner. Extending this basic concept to determine the shielding effectiveness of a metallic screen, however, is complicated by the geometrical periodicity of the mesh which produces a grid work of small apertures. Modern electromagnetic simulation software is not well-suited for that type of problem, and thus a more fundamental approach is necessary. In this section, the transmission loss through the screen as a function of frequency is calculated and compared with measurements at 1.5 and 3.5 GHz.

3.1. Fundamentals

The basic scattering problem formulation is shown in Fig. 2. A Cartesian coordinate system defines the orientation of the mesh cells while the incident electric field orientation is expressed in cylindrical coordinates. Two simplifying assumptions are employed in the following analysis: 1) the mesh is planar, and 2) the wire cross-over junctions are in electrical contact.

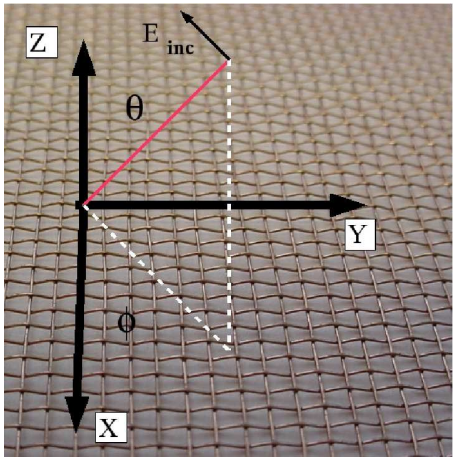

Figure 2. Close-up photograph of the wire mesh with Cartesian and cylindrical coordinate systems superimposed.

The electric field vector of the arbitrarily polarized incident plane wave may be described by

$$\vec{E}_{inc} = \vec{E}_o \, e^{i\omega t} \, e^{ikz \, \cos \, \theta} \, e^{ik(x \, \cos\phi + y \, \sin\phi) \, \sin\theta} \tag{1}$$

where ω is the angular frequency, k is the free space wavenumber, θ is the angle of incidence, and ϕ is the angle subtended by the plane of incidence and the x-directed mesh wires. Currents induced in the wires will scatter the wave thus producing both reflected and transmitted components. The transmission coefficient, which is derived from an analysis of the mesh geometry and the incident wave orientation, will serve as a means to quantify the screen's shielding effectiveness.

While the electromagnetic analysis of parallel wires in free-space dates back to the early 20th century, Kontorovich (1963) and his colleagues (Kontorovich *et al.* 1962) were the first to analyze the mesh problem, beginning in the early 1960's. They developed what has become known as the Average Boundary Condition Method where the electric Hertz vector in terms of the free-space Green's function and an averaged current density over a square mesh cell is integrated to obtain the smoothed electric field on both sides of the screen. A quadratic polynomial approximation for the currents on the wires within each cell is assumed and not derived from the incident field. The polynomial coefficients are found by imposing Kirchoff's law at the junction points and assuming that the charge density is continuous across the junctions. An impedance can also be included between the wires at each junction. It has been demonstrated that this approach produces results that are in good agreement with rigorous methods (Wait 1978), if the mesh cell size is small compared to λ.

One such rigorous approach is the Direct Boundary Value Method developed by Hill and Wait (1976). From Floquet's theorem (Collin 1992), the wire currents can be written as periodic functions multiplied by the phase dependence of the incident field. By setting the total tangential electric field equal to zero at the tops of the wires in the $+z$-direction, a doubly-infinite set of linear equations can be obtained for the spatial Fourier coefficients. This procedure is equivalent to Method of Moments solution of Pocklington's equation for thin wires using entire domain sinusoidal expansion and testing functions (Stutzman and Thiele 1981).

The solution to the doubly-infinite set of equations for the coefficients requires truncation and matrix inversion. Convergence problems arise due to the discontinuity of the currents at the wire cross-over junctions. A "jump function" was developed by Hill and Wait (1976) to get around this problem and its application greatly improved convergence time.

When the cell size is small compared to $\lambda/2$ there are no grating lobes and only the constant current components of the Fourier series contribute to the scattered far field. If the source emitting electromagnetic radiation is located within the $+z$ half-space, then the transmitted fields can be calculated for large -z and a transmission coefficient computed. Similarly, for large $+z$ the reflection field and corresponding reflection coefficient can be determined.

Casey (1977) showed that an analytic solution can be obtained from Wait's results by defining an equivalent sheet impedance tensor relating the space-averaged tangential electric field to the space-averaged surface current density

on the screen as

$$\vec{E}_s \;=\; \mathbf{Z}_s \;\cdot\; \vec{J}_s. \tag{2}$$

This relation is valid if the mesh dimensions are small compared to λ such that only one spatial harmonic is required. Derived from Casey (1988), the impedance tensor in terms of the mesh geometry is given by

$$\mathbf{Z}_s \;=\; Z_{int}\,\mathbf{N} \;+\; X\,\mathbf{G}, \tag{3}$$

where $\mathbf{N}$ is a tensor defined as

$$\mathbf{N} \;\equiv\; \delta_l^k \;-\; \hat{n}_l^k, \tag{4}$$

which is essentially the difference between the Kronecker delta, δ_l^k, and the tensor, $\hat{n}_l^k$, obtained from the direct product of the vector normal to the surface occupied by the mesh with itself.

The tensor operator, $\mathbf{G}$, is defined as the direct product of the ∇ gradient operator with itself or

$$\mathbf{G} \;\equiv\; \nabla\nabla. \tag{5}$$

The coefficient Z_{int} is a complex scalar impedance that is internal to the mesh,

$$Z_{int} \;=\; Z'_w\,a_s \;+\; i\omega L_s, \tag{6}$$

while the coefficient X, which is a reactance due to the reaction field, is

$$X \;=\; \frac{i\omega L_s}{2k^2\hat{\epsilon}_r}, \tag{7}$$

where the sheet inductance parameter, L_s, is given by Casey (1988),

$$L_s \;=\; \frac{\mu_o\,a_s}{2\pi}\ln(1-e^{\frac{-2\pi r_w}{a_s}})^{-1}. \tag{8}$$

The a_s variable is the mesh wire spacing and r_w is the wire radius. From Ramo *et al.* (1965), the internal impedance per unit length of wire, Z'_w, is given by

$$Z'_w \;=\; R'_w\frac{\sqrt{i\omega\tau_w}\,I_o\,(\sqrt{i\omega\tau_w})}{2\,I_1(\sqrt{i\omega\tau_w})}, \tag{9}$$

where $R'_w = (\pi\,r_w^2\,\sigma_w)^{-1}$ is the dc resistance per unit length of the mesh wires, $\tau_w \;=\; \mu_w\,\sigma_w\,r_w^2$ is the diffusion time constant, and $I_n(\cdot)$ denotes the modified Bessel function of the first kind of order n. σ_w and μ_w are the conductivity and the permeability of the wire material, respectively. $\hat{\epsilon}_r$ is an averaged permittivity for the dielectric in which the mesh is embedded and is unity for air.

If we place our coordinates as shown in Fig. 2, $\mathbf{Z_s}$ in Eqn. (3) can be written in matrix form as

$$\mathbf{Z_s} \;=\; \begin{bmatrix} Z'_w a_s \;+\; i\omega L_s\left(1+\frac{1}{2k_o^2\hat{\epsilon}_r}\,\frac{\partial^2}{\partial x^2}\right) & i\omega L_s\left(1+\frac{1}{2k_o^2\hat{\epsilon}_r}\,\frac{\partial^2}{\partial x\partial y}\right) \\ i\omega L_s\left(1+\frac{1}{2k_o^2\hat{\epsilon}_r}\,\frac{\partial^2}{\partial x\partial y}\right) & Z'_w a_s \;+\; i\omega L_s\left(1+\frac{1}{2k_o^2\hat{\epsilon}_r}\,\frac{\partial^2}{\partial y^2}\right) \end{bmatrix} \tag{10}$$

Evaluating the matrix eigenvalues we find

$$Z_{s1} \;=\; Z'_w a_s + i\omega L_s, \tag{11}$$

and

$$Z_{s2} \;=\; Z'_w a_s + i\omega L_s \;+\; \frac{i\omega L_s}{2k_o^2 \hat{\epsilon}_r}\nabla_s^2 \;=\; Z_{s1} - \frac{i\omega L_s}{2}\sin^2\theta, \tag{12}$$

where ∇_s^2 is the two-dimensional Laplacian operator applied to the mesh surface. It can be shown (Casey 1988) that a unique surface current density eigenvector corresponds to each of the two sheet impedance eigenvalues. Z_{S1} and its current density are related to fields that are transverse-electric (TE) with respect to the mesh surface normal and Z_{S2} to the transverse-magnetic (TM) fields. The geometry of these two modes may be visualized with the aid of Fig. 3.

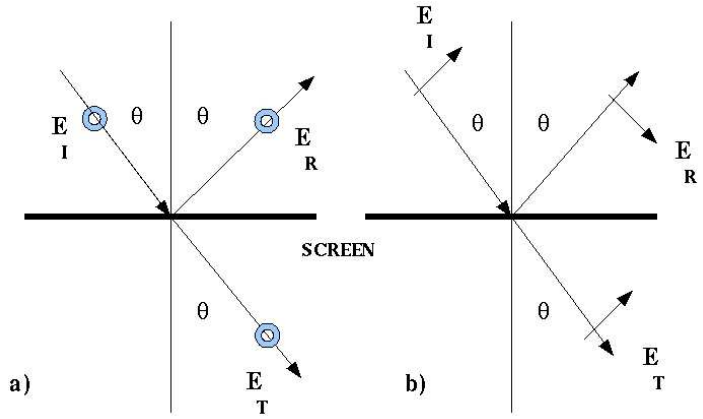

Figure 3. The geometry for the two modes of oblique incidence. Shown are plane waves having a) perpendicular polarization and b) parallel polarization with respect to the plane of incidence.

The problem of determining the effectiveness of a screened enclosure can be addressed by way of a transmission line analogy (Adler *et al.* 1960), as illustrated in Fig. 4. The screen produces a shunt circuit element characterized by the sheet impedance, Z_{S1} or Z_{S2}, between two transmission lines having characteristic impedances Z_1 and Z_2 and propagation constants β_1 and β_2, respectively. These impedances are affected by the incidence angle as

$$Z_1 \;=\; Z_2 \;=\; \frac{Z_o}{\cos\theta}, \tag{13}$$

and

$$\beta_1 \;=\; \beta_2 \;=\; \beta_o \cos\theta, \tag{14}$$

where Z_o and β_o are the intrinsic impedance and propagation constant of free space, respectively.

A wave that is perpendicularly polarized to the plane of incidence and propagating from left to right along the first transmission line would encounter

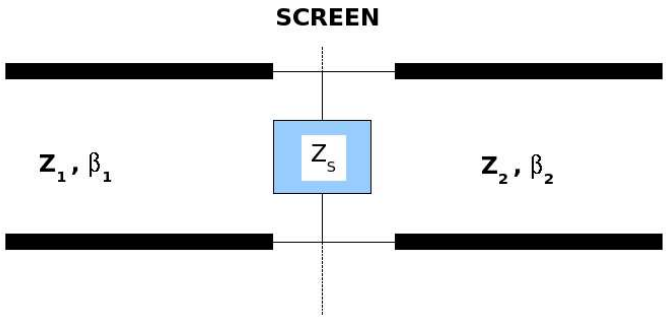

Figure 4. Transmission line model for the problem of plane-wave incidence on a wide mesh screen.

a reflection at the screen, characterized by the coefficient

$$\Gamma_1(\omega,\theta) \;=\; \frac{\frac{Z_2 Z_{S1}}{Z_2+Z_{S1}} - Z_1}{\frac{Z_2 Z_{S1}}{Z_2+Z_{S1}} + Z_1}, \tag{15}$$

and, after some algebra,

$$\Gamma_1(\omega,\theta) \;=\; \frac{-1}{1+2(Z_{S1}/Z_o)\cos\theta}. \tag{16}$$

The transmission coefficient, T, is

$$T_1(\omega,\theta) \;= 1-\Gamma_1 \;=\; \frac{2(Z_{S1}/Z_o)\cos\theta}{1+2(Z_{S1}/Z_o)\cos\theta}. \tag{17}$$

Similarly, for parallel polarization,

$$\Gamma_2(\omega,\theta) \;=\; \frac{\frac{Z_2 Z_{S2}}{Z_2+Z_{S2}} - Z_1}{\frac{Z_2 Z_{S2}}{Z_2+Z_{S2}} + Z_1} \;=\; \frac{\cos\theta}{2(Z_{S2}/Z_o)+\cos\theta}, \tag{18}$$

and

$$T_2(\omega,\theta) \;= 1-\Gamma_2 \;=\; \frac{2(Z_{S2}/Z_o)}{2(Z_{S2}/Z_o)+\cos\theta}. \tag{19}$$

Both are consistent with Casey (1988). The shielding effectiveness as a function of frequency can now be determined for a specific mesh material by calculating the transmission loss through the screen as

$$SE_{1,\,2}(\omega,\theta) \;=\; -20\log_{10}|T_{1,\,2}(\omega,\theta)|, \tag{20}$$

where the transmission coefficient is given by eqns. (17) and (19) for the two E-field polarization cases.

Figure 5. Photograph of the two waveguide test fixtures for measuring the transmission through the screen. The larger one is for 1.5 GHz and the smaller for 3.5 GHz.

3.2. Shielding Effectiveness

The screen's shielding effectiveness was evaluated by way of an insertion measurement in WR-650 waveguide at 1.5 GHz and WR-229 waveguide at 3.5 GHz. The fixtures are shown in Fig. 5. A sample of the screen was clamped between the flanges located part way along the guide. An Agilent 8753D Vector Network Analyzer was used to measure $|S_{21}|$, which can be compared directly to Eqn. (20). Although the calibration was performed at the coaxial ports, the error is less then 0.3 dB. Measured values of $|S_{21}|$ as a function of frequency are shown in Fig. 6.

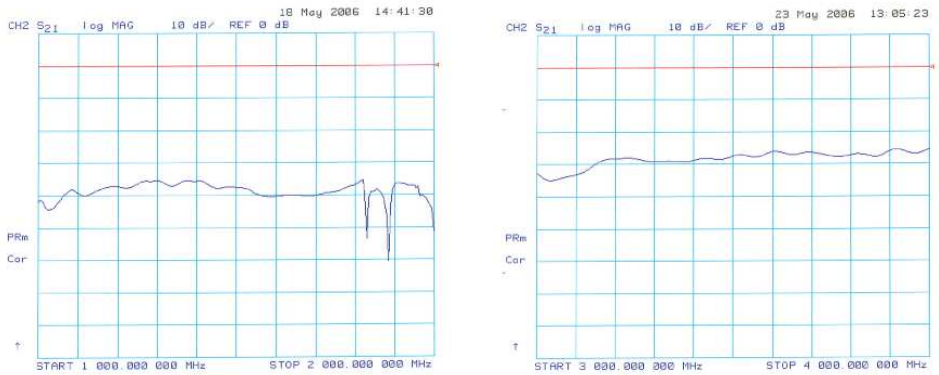

Figure 6. Measured $|S_{21}|$ versus frequency for the wire screen in the two test fixtures shown in Fig. 5. Vertical scale is 10 dB per division with the reference line (red) at 0 dB. Higher order moding is seen above 1.8 GHz

Mathcad software was utilized to calculate the transmission loss through the given mesh as a function of frequency as per Eqn. (20), and the results are presented in Fig. 7. The E-field is oriented in the direction of 18-holes per inch in the mesh. The agreement between theory and measurement is within one percent. Note that $SE_1(\omega, 0) = SE_2(\omega, 0)$ for .the waveguide case, but this is not generally true for oblique incidence. For the situation where the polarization may be random, Casey goes on to define a polarization-independent shielding

effectiveness as

$$SE_o(\omega,\theta) \;=\; -10\log_{10}\left[\frac{1}{2}|T_1(\omega,\theta)|^2+\frac{1}{2}|T_2(\omega,\theta)|^2\right]. \tag{21}$$

Equation (21) may be used to calculate the attenuation of emissions generated within a very large screened enclosure. However, the enclosure described here behaves as a waveguide that is terminated on both ends by the sheet impedance of the screen wire. The resulting structure forms a cavity resonator that sports an undesirable effect when used to contain RF power. This situation will be analyzed in the next section.

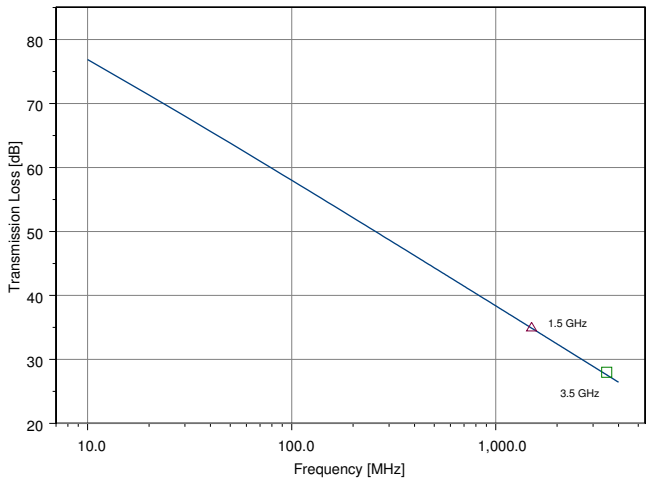

Figure 7. Plot showing calculated transmission loss versus frequency for a TE-mode wave at normal incidence ($\theta = 0$) to the mesh (as in the case of fundamental mode waveguide propagation). Measured values at 1.5 GHz and 3.5 GHz are also shown. E-field is oriented in the direction of 18-holes per inch in the mesh.

4. Resonant Cavity Effect

4.1. Fundamentals

The screened enclosure shown in Fig. 1 is actually a cavity resonator. A waveguide version of this cavity was fabricated to study its characteristics using network analysis techniques. A photograph and sketch of the fixture is shown in Fig. 8. It consists of three sections of WR-229 rectangular waveguide terminated with coaxial-to-waveguide transitions on both ends. The central section forms a resonator when metallic screening is placed at its flanges. The E-field is oriented in the 18-holes per inch direction. The screen also serves to weakly couple the resonator to the transmission line. An equivalent circuit model for this network is given in Fig. 9. The propagation constant, β_{mn}, is given as

$$\beta_{mn} \;=\; \sqrt{\left[\frac{2\pi}{\lambda_o}\right]^2-\left[\frac{m\pi}{a}\right]^2-\left[\frac{n\pi}{b}\right]^2}, \tag{22}$$

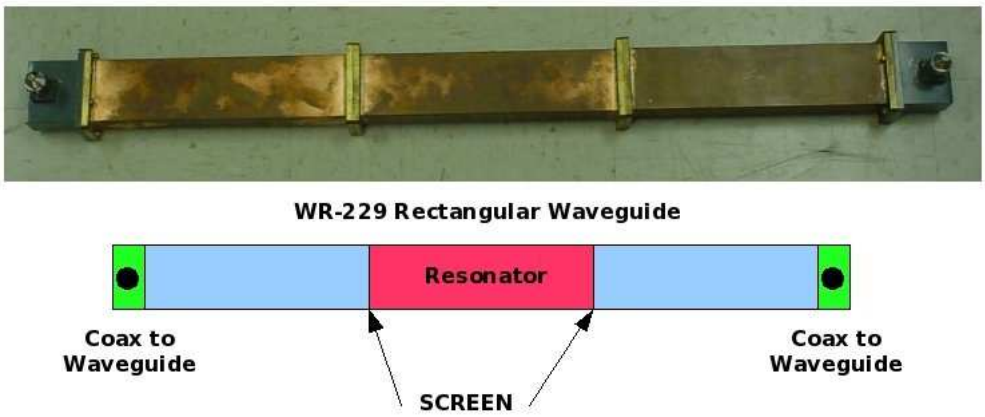

Figure 8. Photograph and sketch of the resonator test fixture.

where λ_o is the free space wavelength, a and b are the width and height of the waveguide, and m and n are integers. In this case, $a = 5.78$ cm and $b = 2.89$ cm for WR-229. The guide impedance for the TE-mode is

$$Z_{TE}(f) \;=\; 2\pi f \sqrt{\mu_o \epsilon_o}\, \frac{377}{\beta_{mn}}, \tag{23}$$

where f is the frequency. The equivalent impedance of the cavity resonator can be found by combining the sheet impedances of the two screens together with the intervening length of waveguide. The guide transforms the sheet impedance on the right (see Fig. 9) to

$$Z_a(f) \;=\; Z_{TE}(f) \frac{Z_{s1}(f)\cos(\beta_{mn} d) + i Z_{TE}(f)\sin(\beta_{mn} d)}{Z_{TE}(f)\cos(\beta_{mn} d) + i Z_{s1}(f)\sin(\beta_{mn} d)} \tag{24}$$

where d, the length of the resonator, is 24.9 cm in this case. A derivation of (24) can be found in Johnk (1975). Z_a(f) is combined with the sheet impedance on the left (Fig. 9) to obtain the cavity impedance as

$$Z_{cavity}(f) \;=\; \frac{Z_a(f) Z_{s1}(f)}{Z_a(f) + Z_{s1}(f)} \tag{25}$$

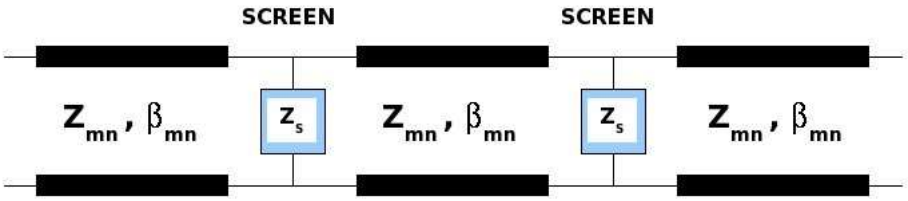

Figure 9. Network model of the resonator.

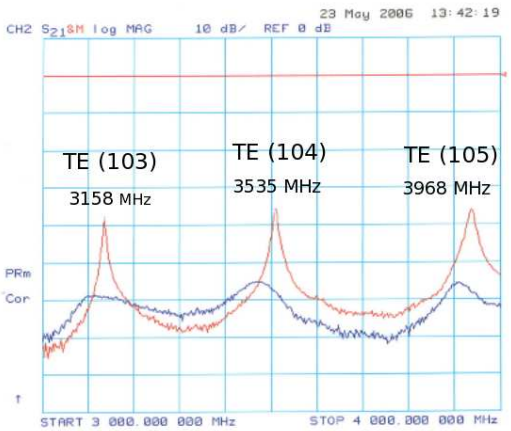

Figure 10. Measured $|S_{21}(f)|$ for the WR-229 cavity resonator (blue: slightly loaded, red: unloaded). Calculated values for the resonant frequencies of the unloaded cavity are also given.

The imaginary part of the denominator in Eqn. (25) vanishes at the resonant frequencies where the cavity impedance becomes real-valued. Fig. 10 shows the measured frequency response obtained using the Agilent 8753D Vector Network Analyzer (red curve) together with the calculated resonant frequencies determined by evaluating Eqn. (25) using Mathcad. The measured frequencies of the peaks in $|S_{21}|$ are within one percent of the calculated values. Note that at the resonant frequencies of the cavity there is more energy passing through two screens than is indicated by Eqn. (20)! The multiple reflections of the wave at resonance add coherently at the screen and correspondingly enhance the transmission through them. Thus, the screen's shielding effectiveness at those frequencies is seriously compromised.

One solution to this problem is to load the cavity with absorbing material. A small amount of Plastazote LD32CN [1] (5 x 20 x 118 mm) was placed on the center line along the broad wall of the waveguide. This absorber, which has a complex dielectric constant, effectively reduces the amplitude of the reflected waves and alters the propagation constant. This is illustrated by the blue curve in Fig. 10. The Q is reduced significantly, and the resonant frequencies are lowered. By covering the entire broad wall of the waveguide with a thin slab of Plastazote LD32CN (5 x 58 x 164 mm) the resonant enhancement effect is virtually eliminated, as shown in Fig. 11 (blue curve).

4.2. Measured Shielding Effectiveness of the Screened Enclosure

The effectiveness of the enclosure to contain RF emissions was measured in the anechoic chamber at the NRAO facility in Green Bank, WV by C. Beaudet. The box was located approximately seven meters from the log-periodic receive antenna (EM-6950). The received signal was amplified (Miteq AM-4A-000110-N-1306/E) and sent to a spectrum analyzer (Antitsu MN MS2602A) for detection.

[1] Plastazote is a registered trademark of Rubberlite Inc., Huntington, WV

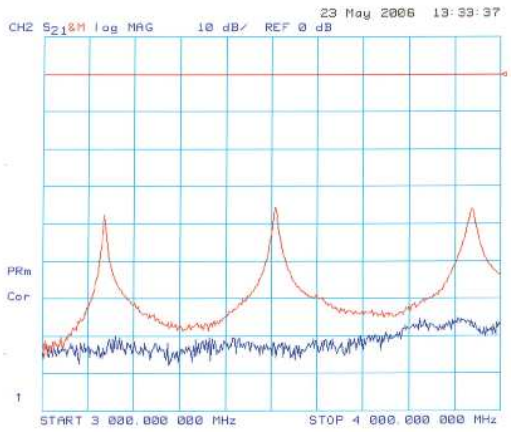

Figure 11. Measured $|S_{21}(f)|$ for the WR-229 cavity resonator. (red) unloaded and (blue) loaded with a thin slab of absorbing material along the entire broad wall of the cavity.

The analyzer was swept from 30 - 1000 MHz in thirty seconds with a resolution bandwidth of 10 kHz. The output was averaged over several sweeps to obtain the spectral curve.

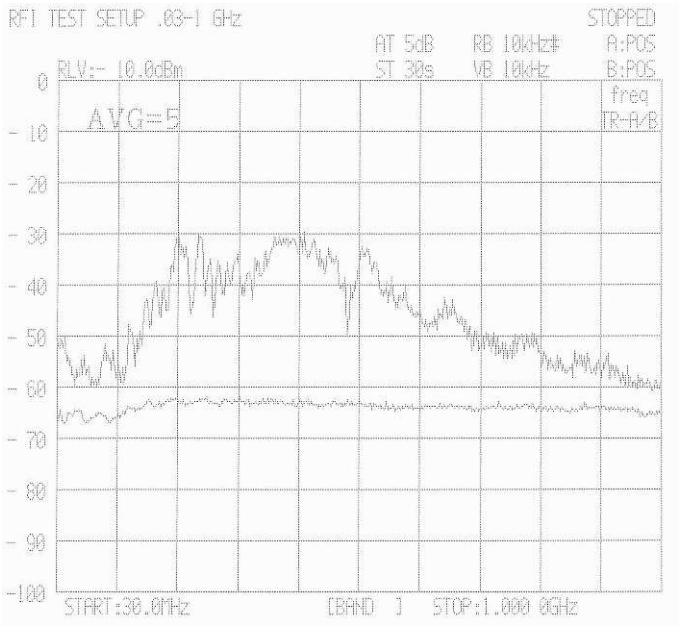

Figure 12. Measured power versus frequency for the noise source located inside the open screen box. The chamber background level is also shown.

The noise source used in these measurements was a child's light toy that contains a dc motor that spins several flashing LEDs at a few hundred rpm. This device generates a significant amount of energy over the 30-1000 MHz band as shown in Fig. 12. This plot also includes the chamber background level for reference.

The shielded box was then closed, the lid held in place with a set of wood screws spaced approximately four inches apart. The swept frequency measurement reveals a significant attenuation of the noise source, but the transmission-enhancement effect caused by the cavity resonances is clearly visible in Fig. 13. Again, Eqn. (25) was employed to calculate the resonant frequencies, which

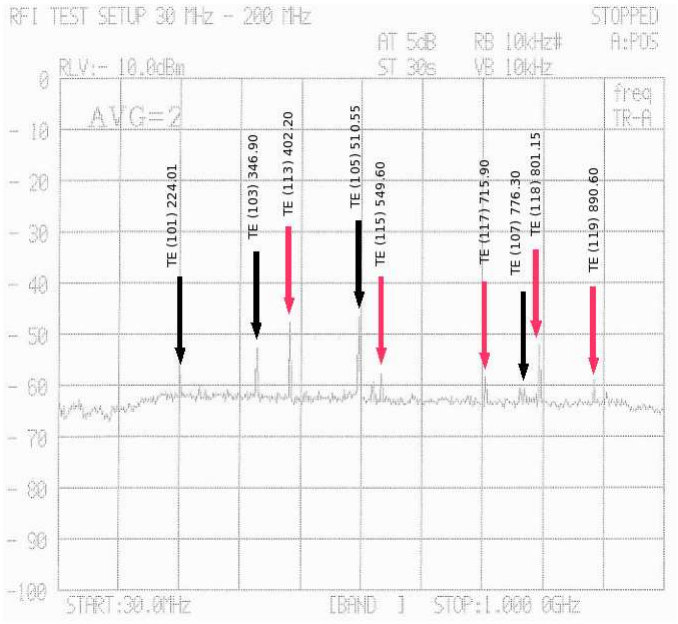

Figure 13. Measured power versus frequency for the noise source located inside the screen box with the lid fastened. Calculated frequencies for nine of the TE-10n (black) and TE-11n (red) resonances are shown. n is an integer.

align very nicely with the measurements. A near- field RF probe connected to a spectrum analyzer confirmed that the leakage was through the mesh and not at the seams.

Two sheets of Plastazote LD32CN were cut to cover the entire bottom of the shielded box to form an absorber approximately 2.6 inches thick. As shown in Fig. 14, the absorber attenuates the Q of the cavity and effectively reduces the RF leakage to the background reference level shown in Fig. 12.

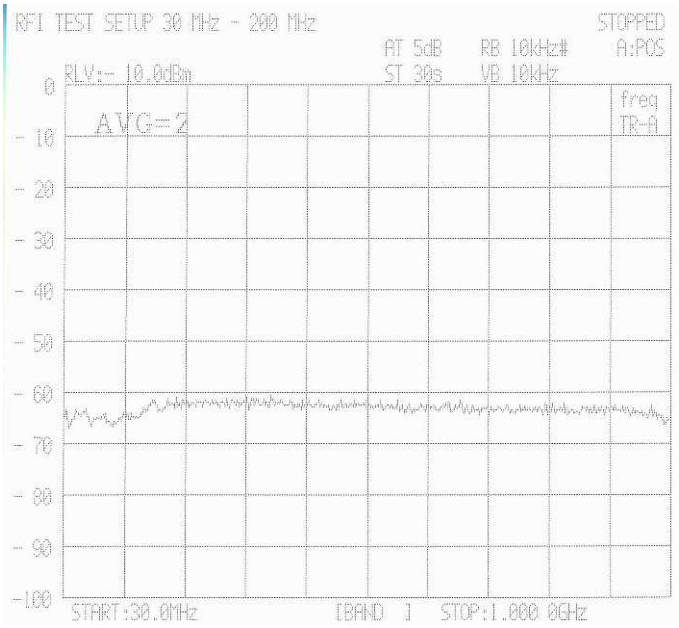

Figure 14. Measured power versus frequency for the noise source located inside the screen box with the lid fastened. The box also contained two sheets of Plastazote covering the entire bottom. Compare result with background level in Fig. 12

5. Applications

5.1. Shielding Electronic Equipment

One direct application for this enclosure is to shield high-speed signal processing equipment from sensitive receiver electronics. A case in point is the instrument know as the Precision Array to Probe the Epoch of Reionization (PAPER). An array of sleeved dipoles for 130-200 MHz surrounds a central hut which contains FPGA-based digital correlation equipment being clocked at 600 MHz.

The correlator for PAPER uses technology developed at the Berkeley Wireless Research Center (BWRC) and employed by the Center for Astronomical Signal Processing and Engineering Research (CASPER) group. The sub-system for which the EMC measurement results are presented here includes one Internet Break-Out Board (IBOB) which contains two Fourier spectrometers, two dual-channel A/D converter boards, a synthesized signal generator, switching power supplies, and a laptop computer. Fig. 15 shows the measured power spectral density of the radio emissions with the shielded enclosure open. Fig. 16 shows the emissions when the lid is firmly in place. The shielding effectiveness follows the curve in Fig. 7.

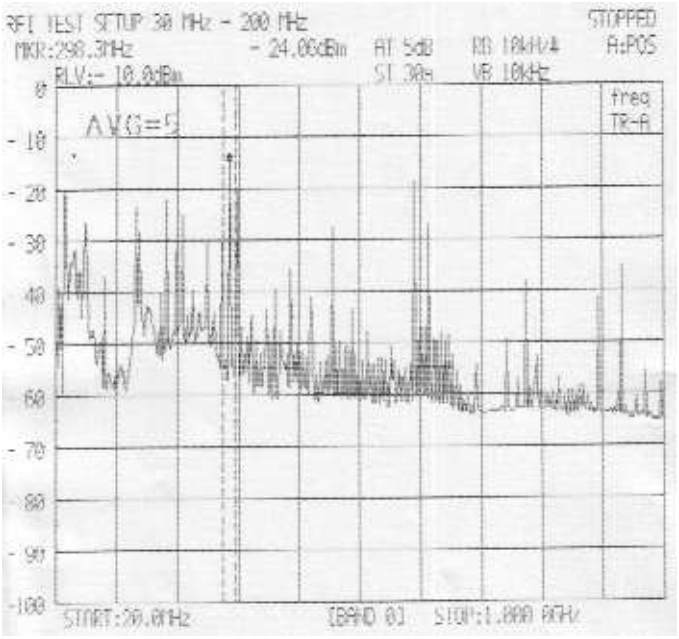

Figure 15. Measured power versus frequency for components of the PAPER digital sub-system located in the anechoic chamber. Shielded box was open.

5.2. Demonstrator

The enclosure was used during the NRAO Charlottesville Open House to demonstrate how metallic screening is used to isolate sensitive electronic equipment from the electromagnetic environment. It can also illustrate several basic principles of electromagnetics as well as contrast the physical characteristics of electromagnetic and pressure waves.

A portable FM broadcast radio tuned to a strong station is placed inside the enclosure. With the lid off the enclosure sound waves demodulated from the station's signal can be heard emitting from the radio's speaker. However, with the lid in place the radio station's signal is attenuated according to the curve in Fig. 7 and only the faint background noise of the receiver electronics can be heard from the speaker.

6. Conclusions

There are three fundamental conclusions that can be drawn from this work:

- The physical size of the enclosure should be just large enough to house the electronic equipment. This will increase the cutoff frequency of the cavity.

- Absorbing material is required inside the enclosure to reduce the enhanced radiation caused by the cavity resonance effect.

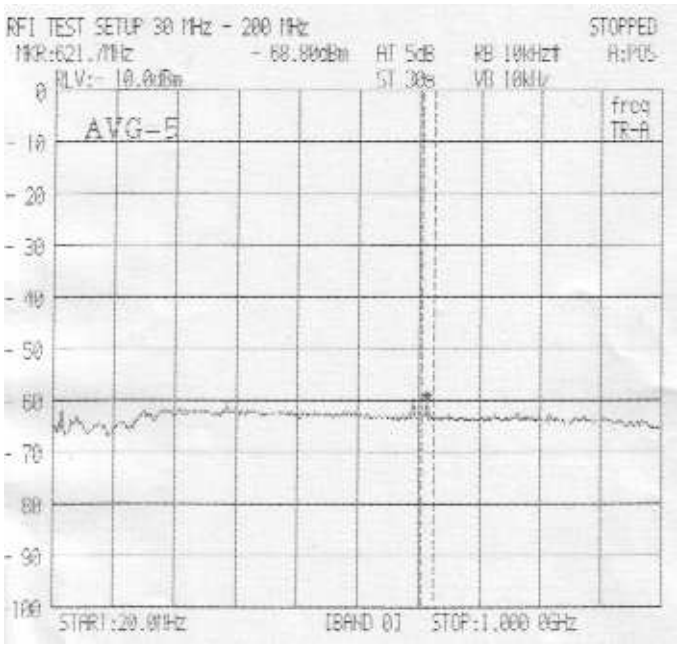

Figure 16. Measured power versus frequency for components of the PAPER digital sub-system located inside the shielded enclosure located in the anechoic chamber. The shielded box was closed.

- The physical size of the mesh will affect the amount of energy that can pass through it as a function of frequency. Therefore, the spectral density of the RF emissions generated by the electronic equipment should be considered when choosing the mesh size.

7. Acknowledgments

I would like to thank C. Beaudet for performing the RFI measurements involving the anechoic chamber in Green Bank and D. Boyd for many useful discussions during fabrication. I also thank E. Mastrantonio for proof-reading the manuscript.

A Appendix - Enclosure Assembly Details

Assembly details are provided below. Note that the given dimensions are for the enclosure that was investigated in this study. The size of the enclosure will affect the resonant frequencies of the cavity, but since the absorber mitigates the enhanced transmissions, the physical dimensions can therefore be set by the size of the equipment to be shielded. Emphasis is placed on those features of the box that influence shielding effectiveness.

A1. Materials List

- white pine boards: 2" x 4" x 8' - 8 pieces.
- 18 x 14 wire mesh: bright bronze, 0.011" dia. wire, 36" x 26'.
- copper gauze: 5" wide x 48' length.
- gasket rope seal: 5/16" dia., 48' length.
- wood screws: No. 8, 2.5" length, coated steel - approx. 300.
- wood screws: brass, No. 5, 3/4" length - approx. 70.
- copper plates, 3/32" thick, 1' x 2', - 2 pieces.
- staples: 3/8" tall.
- dowel rod: poplar, 1/8" dia. 3' length, - 4 pieces.
- wood adhesive.

A2. Assembly Instructions

Material preparation begins with the wooden pieces that make up the structural framework. All of these pieces have a 1.5" square cross-section. The 2" x 4" x 8' stock is first cross-cut to the appropriate lengths and then ripped to produce (4)-12", (8)-29", (4)-30.5", (16)-32", (6)-63", and (2)-66" pieces. The 3/4" deep, 1.5" wide notches are cut at the locations of the double-lap joints, as illustrated in Sec. A4. The 1/8" dia. through-holes for the dowels were drilled in accordance with the detail drawing shown in Fig. 17. A jig was made to provide a means of locating these holes quickly. The frame pieces that make up the two ends and top of the enclosure receive a series of 3/16" dia. through-holes for wood screws and a 3/8" wide groove for the rope seal. Do not include the through-holes in the wood pieces that secure the bulkhead. Details are provided in Fig. 18. Finally, the dowels are cut into pieces of length 1.375".

Assembly begins by fabricating the bottom, top, sides, and ends of the enclosure separately. The various wood pieces required are as follows:

- bottom: (2)-63" and (5)-32"
- top: (2)-66" and (3)-32" (includes milling for rope seal)
- side *A*: (2)-63" and (5)-29"
- side *B*: (2)-63" and (3)-29"
- each end: (4)-32", (2)-30.5", and (2)-12" (includes milling for rope seal)

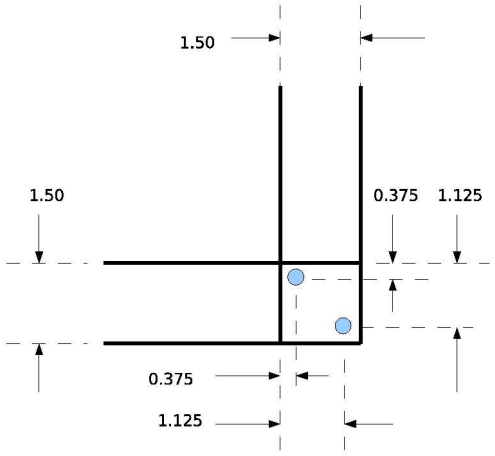

Figure 17. Detail of the double-lap joint showing the location of the dowels.

The assembly procedures are similar for each section of the enclosure. Four 90-degree corner clamps are used to hold the outer pieces squarely in place on a flat surface. A hand drill is used to transfer the dowel holes from the upper to the lower parts of the double-lap joints. The corner clamps are loosened, wood adhesive is added to the mating surfaces of the joint, and the pieces re-assembled. Dowels are lightly tapped into place, the corner clamps are tightened, and compression clamps are added to apply pressure to the lap joints. All clamps are removed after allowing appropriate time for the adhesive to set. The inner pieces of wood that form the support ribs are then attached to the frame in a similar manner, but the corner clamps are not necessary.

The two sides of the enclosure are attached to the bottom frame as shown in Fig. 1. Note that the sides rest on top of this frame and are secured by the No. 8 wood screws located 3.5" to either side of the ribs. Detail of the milled groove for the rope seal and locations of the 3/16" dia. through-holes for the No. 8 screws are shown in Fig. 18.

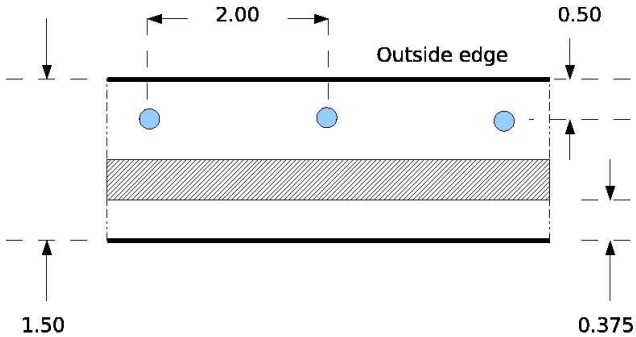

Figure 18. Detail of the milled 3/8" wide groove for the rope seal and positions of the through-holes for the No. 8 wood screws.

On the top- and end-sections of the enclosure, a small amount of material between the adjacent milled slots must now be removed so that a continuous pathway exists for the rope seal. The seal is placed in the slot to determined the overall length; it is cut and then removed. A small amount of wood adhesive is placed in the bottom of the slot and the seal re-inserted. Note that the bulkhead support pieces on the ends of the enclosure also require the seal.

Next, the mesh is cut to the appropriate dimensions. For the top and ends of the enclosure the mesh is cut 1/4" shorter than the framework dimensions allowing for a 1/8" recess all around. For the sides and bottom, two pieces 36" x 90" are cut and a splice is made by folding back 2" of mesh along the long dimension and overlapping them with a piece of copper gauze in between. The pieces are positioned on the inside of the framework and secured by staples. A series of closely spaced staples are fastened through the overlapped mesh along the central rib of the sides and bottom to secure the splice to the frame. Be sure the mesh folds around the framework on the top and ends to provide enough material for electrical contact with the corresponding framework sections. Trim the mesh so that it is recessed by 1/8" along the edges.

The top and ends of the enclosure also require the copper gauze to form an electrical gasket. This is accomplished by folding the 5" wide gauze strip in half and stapling the open ends of it to the framework over the rope seal. This gauze is also used around the bulkhead.

Final assembly of the enclosure requires that the ends be attached to the sides and bottom structure using the No. 8 wood screws. Care must be taken to ensure that the copper gauze is not kinked. The mesh is cut away in the bulkhead regions and the copper bulkhead plates are attached from the inside using No. 5 brass wood screws. The top of the enclosure can now be put in place, secured by No. 8 wood screws to complete the assembly.

A3. Improvements

We have made a few improvements to the enclosure based upon lessons learned from fabricating and operating the original. The wood screws used to attach the lid were found to easily tear the copper gauze. Furthermore, some of the screw threads in the white pine were stripped after only a few cycles of opening and closing the lid. We have replaced these screws with "tee" nuts and bolts on newer designs. We also found that the spacing of two inches for the wood screws on the lid was overly conservative since the copper gauze works very well to fill voids at the interface. Therefore, we increased the bolt spacing to six inches.

A4. Mechanical Drawings

The following is a set of mechanical drawing of the enclosure. All dimensions are in inches. Drawings are NOT to scale.

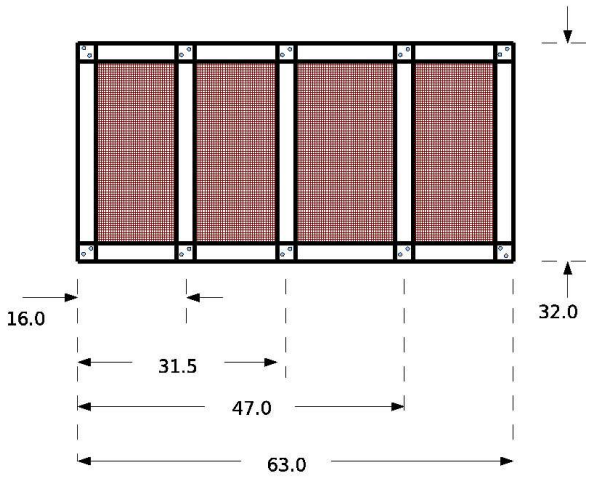

Figure 19. Mechanical drawing of the bottom of the enclosure.

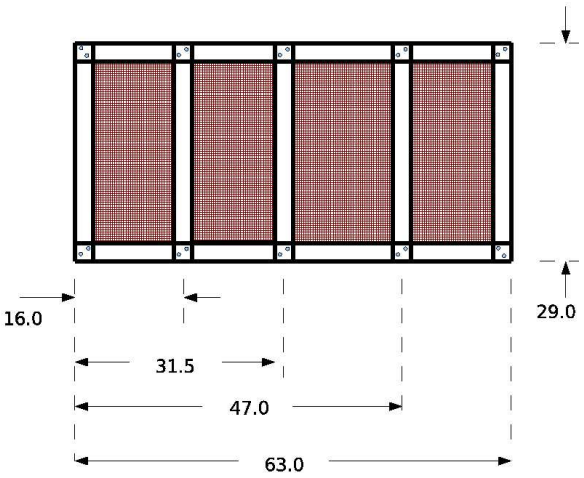

Figure 20. Mechanical drawing of the sides of the enclosure. Side A has all five vertical pieces while side B has only three.

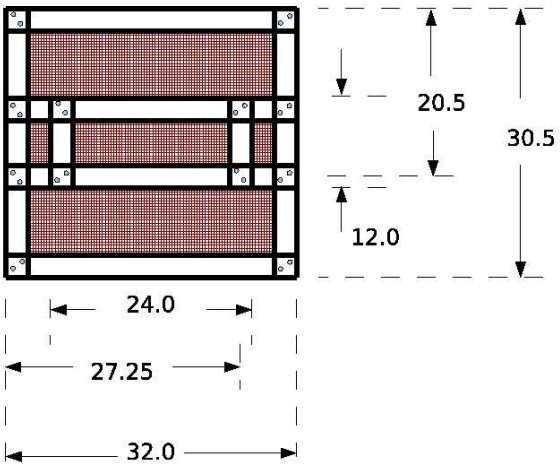

Figure 21. Mechanical drawing of the ends of the enclosure showing placement of the bulkheads.

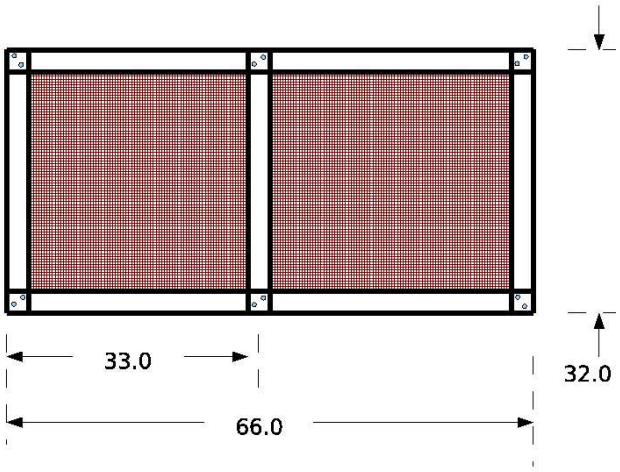

Figure 22. Mechanical drawing of the top (lid) of the enclosure.

References

Adler, R. B., L. J. Chu, and R. M. Fano, Electromagnetic Energy Transmission and Radiation, Wiley, New York, pp. 354-369, 1960.

Beaudet, C., C. Clark, C. Niday, F. Ghigo, J. Ford, R. McCullough, W. Sizemore, and P. Woody, "The Green Bank Interference Protection Group: Policies for RFI Management," Internal Report, Nov. 15, 2005.

Casey, K. F., "Electromagnetic Shielding by Advanced Composite Materials," Air Force Weapons Lab. *Interaction Notes*, C. E. Baum, Ed. Note 341, June 1977.

Casey, K. F., "Electromagnetic Shielding Behavior of Wire-Mesh Screens," IEEE Trans. on Electromagnetic Compatibility, Vol. 30, No. 3, pp. 298-306, 1988.

Collin, R. E., Foundations for Microwave Engineering, 2nd Ed., McGraw-Hill, New York, pp. 569-571, 1992.

Hill, D. A. and J. R. Wait, "Electromagnetic Scattering of an Arbitrary Plane Wave by a Wire Mesh with Bonded Junctions," Canadian J.of Phys., Vol. 54, pp. 353-361, 1976.

Johnk, C. T. A. Engineering Electromagnetic Fields and Waves, Wiley, New York, p. 564, 1976.

Kontorovich, M. I., V. Yu. Petrun'kin, N. A. Yesepkina, and M. I. Astrakhan, "The Coefficient of Reflection of a Plane Electromagnetic Wave from a Plane Wire Mesh," Radio Engineering and Electronic Physics, Vol. 7, pp. 222-231, Feb. 1962.

Kontorovich, M. I. "Averaged Boundary Conditions at the Surface of a Grating with Square Mesh," Radio Engineering and Electronic Physics, Vol. 8, pp. 1446-1454, 1963.

Marcuvitz, N., Waveguide Handbook, Radiation Laboratory Series, No. 10, McGraw-Hill, New York, pp. 238-247, 1951.

Ramo, S., J. R. Whinnery, and T. van Duzer, Fields and Waves in Communication Electronics, Wiley, New York, pp. 295-298, 1965.

Stutzman, W. L. and G. A. Thiele, Antenna Theory and Design, John Wiley, New York, Ch. 7, 1981.

Van Vlack, L. H. Elements of Material Science and Engineering, 4th ed., Addison-Wesley, Reading, MA., p. 475, 1980.

Wait, J. R. "Theories of Scattering from Wire Grid and Mesh Structures,"in Electromagnetic Scattering, P. L. E. Uslenghi, Ed. Academic Press, New York, pp. 253-287, 1978.